Modulation of Substrate–Membrane Interactions by Linear Poly(2-methyl-2-oxazoline) Spacers Revealed by X-ray Reflectivity and Ellipsometry

Peter C. Seitz,[a] Michael D. Reif,[b] Oleg V. Konovalov,[c] Rainer Jordan,*[b, d] and Motomu Tanaka*[a]

Dedicated to Erich Sackmann on the occasion of his 75th birthday

Hydrated polymer interlayers between planar lipid membranes and solid substrates provide a water reservoir and thus maintain a finite membrane–substrate distance. Linear polymer spacers attached to lipid head groups (lipopolymer tethers) can be used as a defined model of oligo- and polysaccharides covalently anchored on cell surfaces (glycocalyx). They can offer a unique advantage over membranes physisorbed on polymer films (called polymer-cushioned membranes), owing to their ability to control both the length and density of polymer chains. In this study, a lipopolymer tether composed of a stable ether lipid moiety and a hydrophilic poly(2-methyl-2-oxazoline) spacer with a length of 60 monomer units is used to fabricate supported membranes by the successive deposition of proximal (lower) and distal (upper) leaflets. Using specular X-ray reflectivity and ellipsometry, we systematically investigate how the lateral density of polymer chains influences the membrane–substrate interactions. The combination of two types of reflectivity techniques under various conditions enables the calculation of quantitative force–distance relationships. Such artificial membrane systems can be considered as a half-model of cell–cell contacts mediated via the glycocalyx, which reveals the influence of polymer chain density on the interplay of interfacial forces at biological interfaces.

Introduction

Bilayer lipid membranes deposited on planar substrates (supported membranes) have been used intensively for mimicking the structures and functions of biological membranes.[1–3] More recently, polymer-supported membranes have drawn increasing attention as a more sophisticated model for membrane–extracellular contacts that provide soft interlayers for immobilization of membrane proteins without the risk of denaturation.[4,5] Model systems proposed so far can mainly be classified into two categories: 1) supported membranes deposited on preformed polymer films (polymer-cushioned membranes);[6] and 2) supported membranes separated from solid substrates by linear polymer spacers (polymer-tethered membranes).[7–12]

One unique feature that polymer-tethered membranes can potentially offer is the flexible and quantitative control of the membrane–substrate interactions. For example, if the lateral density of lipopolymers can be controlled, the lateral density and thus the volume fraction of polymers in the reservoir between the membrane and the substrate can be precisely adjusted. In our previous account, we demonstrated that the frictional environment surrounding lipids and proteins can be adjusted by the length and lateral density of polymer tethers.[13]

Another interesting aspect of polymer-tethered membranes as compared to polymer-cushioned membranes is the chemical coupling between membrane moieties and the intermediate polymer. As theoretically predicted by Seifert and Merath,[14] the presence of membrane-bound tethers significantly influences their thermodynamic fluctuation, that is, the

interfacial potentials and mechanical properties of the membranes. From the experimental approach, one of the key steps to quantitatively understand the membrane–substrate interaction is the measurement of the thickness and density of polymer interlayers that separate membranes from solid substrates.

To date, there have been several studies on the measurement of the distance between supported membranes and the underlying substrates. For instance, fluorescence interference contrast microscopy (FLIC)[15] is a powerful interferometric tech-

[a] P. C. Seitz, Prof. Dr. M. Tanaka
Biophysical Chemistry Laboratory II
Institute of Physical Chemistry and BIOQUANT
University of Heidelberg, 69120 Heidelberg (Germany)
Fax: (+ 49) 62-21/54-49-18
E-mail: Tanaka@uni-heidelberg.de

[b] M. D. Reif, Prof. Dr. R. Jordan
Wacker-Lehrstuhl für Makromolekulare Chemie
Technische Universität München, 85748 Garching (Germany)
E-mail: Rainer.Jordan@ch.tum.de

[c] Dr. O. V. Konovalov
European Synchrotron Radiation Facility (ESRF)
6 rue Jules Horowitz BP 220, 38043 Grenoble Cedex (France)

[d] Prof. Dr. R. Jordan
Department Chemie, Technische Universität Dresden
01069 Dresden (Germany)
Fax: (+ 49) 3-51/4-63-3-71-22
E-mail: Rainer.Jordan@tu-dresden.de

nique used for the determination of membrane–substrate[16] and cell–substrate[17] distances. However, this measurement relies on many parameters that are sometimes hard to quantify, such as the exact angle of the transition dipole moment of fluorophores with respect to the sample plane. Atomic force microscopy (AFM) operated in a contact mode can merely measure the height difference between the membrane surface and the area scratched under high forces.[18] An alternative way to evaluate the structures of such multilayered systems involves techniques based on reflectivity, such as ellipsometry[19–21] and specular X-ray and neutron reflectivity.[22–27] Taking the basic framework of Fresnel reflectivity, one can calculate the thickness and/or refractive index of the layered structures from the two measured ellipsometric angles.[28] X-ray and neutron reflectivity are performed with much smaller wavelengths, which enables the thickness, scattering length density, and roughness of the buried interfaces to be obtained.

In our previous accounts, we reported that polymer-tethered membranes containing lipopolymers with hydrophilic poly(2-oxazoline) chains can be used for the incorporation of human platelet integrin $\alpha_{IIb}\beta_3$ receptors, and demonstrated that the homogeneity,[10] lateral mobility,[13] and functionality[29] of integrin depends on the spacer length. Herein, we characterize the vertical structures of our polymer-tethered membranes by the combination of ellipsometry and specular X-ray reflectivity. We focus on a lipopolymer composed of an archaea analogue lipid moiety, with ether groups for better chemical stability and isoprenoid tails to avoid alkyl chain crystallization, and a linear hydrophilic poly(2-methyl-2-oxazoline) spacer with sixty monomer units (PMOx60, see Figure 1 and the Supporting Informa-
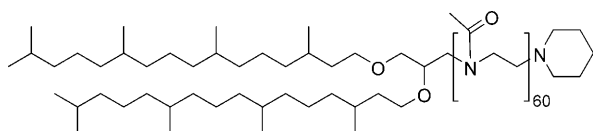
Figure 1. Molecular structure of the lipopolymer tether used in this study (PMOx60).

tion for the chemical structure and name). The lipopolymer was prepared by living cationic ring-opening polymerization to ensure quantitative end-functionalization and a narrow molar mass distribution (polydispersity index, $PDI = M_w/M_n = 1.05$). Asymmetric membranes were prepared in a two-step process: the proximal monolayer with lipopolymers (lower leaflet) is transferred onto the solid substrate by a Langmuir–Blodgett (LB) transfer (Figure 2, left), and the distal monolayer (upper leaflet) is formed by a Langmuir–Schaefer (LS) transfer (Figure 2, right). Details of the obtained results are described in the following sections.

Experimental Section

Materials: Silicon wafers (Si-Mat, Landsberg am Lech, Germany) with native oxide (≈ 15 Å) cut in pieces of approximately 24×20 mm^2 were used as substrates. Deionized water with specific re-
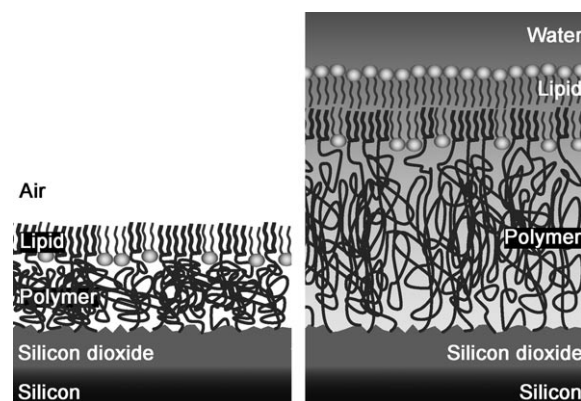
Figure 2. Schematic view of polymer-supported membranes. Left: a dry monolayer with a high concentration of polymer, which is collapsed and very dense. Right: after completion of the bilayer with a Langmuir–Schaefer transfer, the membrane is kept under water. The polymer is swollen and the distance between the silicon substrate and lipid bilayer increases.

sistance $\rho > 18$ MΩ cm (GenPure, TKA, Niederelbert, Germany) was used throughout this study. The substrates were cleaned using a modified RCA protocol:[30] the samples were sonicated for 5 min in acetone, ethanol, methanol, and water, and immersed in a solution of H$_2$O$_2$ (30%)/NH$_4$OH (30%)/H$_2$O (1:1:5 by volume) for 5 min at room temperature before soaking them for another 30 min at 60°C. Afterwards, they were intensively rinsed with deionized water, dried at 70°C, and stored in sealed glass boxes.

1-Stearoyl-2-oleoyl-*sn*-glycero-3-phosphocholine (SOPC) was purchased from Avanti Polar Lipids (Alabaster, AL, USA); other chemicals were from Sigma–Aldrich (Munich, Germany). The lipopolymer used in this study was synthesized according to the previously published route.[10,27,31–34] Since asymmetric membranes were prepared using layer-by-layer transfers, the polymer chain was terminated by a piperidine group instead of a trimethoxysilane surface coupling group to avoid crosslinking by polycondensation.

Membrane Preparation: Both proximal and distal monolayers were first spread on a Nima Langmuir trough Model 311D (Nima, Coventry, England). After checking the cleanness of the subphase by compression and subsequent relaxation of the blank subphase (the change in surface pressure was always below 0.2 mN m^{-1}), a cleaned substrate was immersed into the subphase. The stock solution of lipid/lipopolymer mixture (1 mg mL^{-1} in CHCl$_3$) was deposited on the water surface. After evaporation of the solvent, the film was compressed by moving the barrier at 10 mm min^{-1} up to a surface pressure of 30 mN m^{-1}. Then, the proximal layer was transferred by vertical pulling of the substrate from the water subphase at a constant surface pressure. A high transfer speed of 30 mm min^{-1} was chosen to avoid demixing of the lipid/lipopolymer mixture.[35] Throughout this study, a transfer ratio of unity was guaranteed within the experimental error of ± 2%.

The distal monolayer was deposited onto a monolayer-coated (and thus hydrophobic) substrate by LS transfer: the sample was placed slightly obliquely above the subphase and dropped gently. After floating on the subphase for some seconds, the substrate was pressed into the subphase and transferred to a prismatic cuvette used for ellipsometric measurements without exposing the bilayer to air.

Ellipsometry: A Multiskop instrument (Optrel, Kleinmachnow, Germany) equipped with a He–Ne laser operating at 6328 Å was used

for measurement of the ellipsometric angles ψ and Δ, defined by the ratio of the reflection amplitude coefficients of p- and s-polarized light: $\frac{r_p}{r_s} = \tan(\psi)\exp(i\Delta)$. The beam width of the laser was 1300 μm, which corresponded roughly to a circular footprint sampled for measurement at one spot. Each sample was measured at least at five different spots with zone averaging. The reproducibility of the measurements was checked by successive measurements at the same spot and was found to be limited by the instrumental resolution. The transferred proximal layers were characterized in an atmosphere with relative humidity defined by saturated salt solutions,[36] while the characterization of bilayers was performed under water. A prismatic cuvette (Hellma, Müllheim, Germany) with a 70° angle between the base (substrate) plane and the two observation windows served as the sample environment. The front of the cuvette was sealed with a piece of glass spread with silicone grease (Baysilone silicone paste, low viscosity; Bayer, Leverkusen, Germany). The back reflection of the laser from the cuvette was directed as close as possible to (but not into) the laser exit aperture. Ellipsometric results were evaluated using a self-written code for IGOR Pro (WaveMetrics, Portland, OR, USA) based on the Abelès matrix formalism.[3,28] The fit quality was assessed by evaluating the function of merit [Eq. (1)]:

$$S = \frac{(\Delta_{meas} - \Delta_{model})^2}{\Delta_{model}} + \frac{(\psi_{meas} - \psi_{model})^2}{\psi_{model}} \tag{1}$$

The best parameters resulted in local minima of S. Error estimates were given by parameters that resulted in S being twice the minimum value.

X-ray Reflectivity: Specular X-ray reflectivity measurements were carried out at the ID10b beamline of the European Synchrotron Radiation Facility (ESRF, Grenoble, France). All the measurements were performed at 20 °C in ambient atmosphere, that is, a relative humidity (RH) of about 70%. The radiation energy was $E = 20$ keV. The beam width was set to 300 μm. In the beam direction, the illuminated area decreased from the maximum extension of the sample (20 mm) down to approximately 1.5 mm. The raw data were corrected for over-illumination and normalized below the critical angle. Large changes in the probed area and the aspect ratio had no effect on the measured data, since the homogeneity of the membrane validated the use of a layer model without structures in the membrane plane. The data were analyzed using MOTOFIT running on IGOR Pro.[37]

Results

Characterization of the Monolayer in Air

Prior to the LB transfer of the proximal monolayer, the thickness of the native oxide was determined to be $d_{SiO_2} = (13.8 \pm 1.1)$ Å by assuming refractive indices for silicon and silicon dioxide of $n_{Si} - ik_{Si} = 3.882 - 0.019i$ and $n_{SiO_2} = 1.457$, respectively.[38] Since this value shows a small deviation, this thickness was used as a constant throughout this study. As a reference, we measured the thickness of a pure transferred phospholipid (SOPC) monolayer containing no PMOx60 lipopolymers. Here, we employed a two-slab model that consists of silicon dioxide and lipid monolayer. Assuming the refractive index of lipid to be $n_{lipid} = 1.44$,[39] the thickness of the monolayer was calculated to be $d_{monolayer} = (18.1 \pm 1.3)$ Å. For the monolayers containing PMOx60 lipopolymers, an additional polymer layer between

the silicon dioxide and the lipid monolayer should be taken into account. Within this three-layer model, both the refractive index and thickness of the polymer layer were fitted while keeping the parameters for the other two layers constant (Table 1).

Table 1. Layer model used for ellipsometric measurements on dry monolayers showing the layer thickness d, the real part of the refractive index n, and the imaginary part k.[a]

Layer	d [Å]	n	k
Air	∞	1	0
Lipid	18.1	1.44	0
Polymer	d_{pol}	n_{pol}	0
SiO$_2$	13.8	1.457	0
Si	∞	3.882	−0.019

[a] The parameters for the lipid layer were obtained from a reference measurement on a pure SOPC monolayer prepared under the same conditions. The illumination wavelength is $\lambda = 6328$ Å and the incident angle on the substrate $\Theta = 70°$. The parameters for the polymer layer n_{pol} and d_{pol} were used as fitting variables and best results are shown in Table 2.

The ellipsometric angles ψ and Δ obtained for the transferred monolayers with different molar fractions of PMOx60 at varying humidity are plotted in Figure 3. The increase in poly-
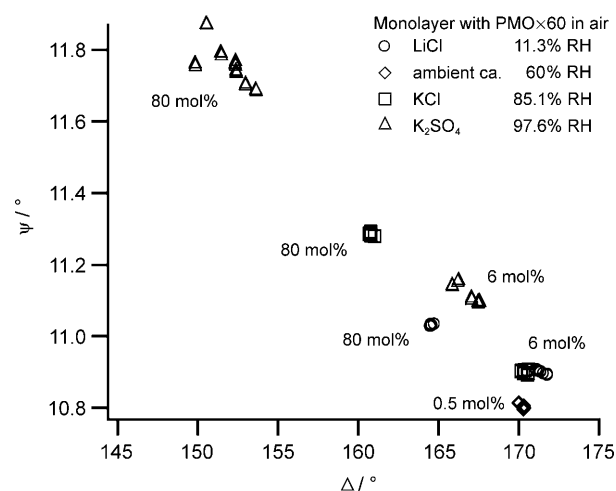
Figure 3. ψ versus Δ plot of selected ellipsometric measurements on dry monolayers doped with PMOx60 on silicon substrates. Each sample was measured under each condition on at least five different spots. The samples were placed in different ambient conditions with saturated salt solutions (denoted by symbol shape) to adjust the relative humidity. The small scatter of data shows the lateral homogeneity of the monolayer, which decreases upon swelling.

mer fraction leads to a monotonic increase of ψ and a decrease of Δ caused by the increase in the humidity from 11% to 98%, which corresponds to the more significant swelling of polymers at higher lateral densities. On the other hand, as presented in Table 2, the thickness of the polymer layer shows a continuous increase in accord with an increase of the lipopolymer concentration from 0 Å (0 mol%) to a maximum of 84.4 Å

Table 2. Refractive index n_{pol} and layer thickness d_{pol} for the polymer layer determined by fitting the model shown in Table 1.[a]

Concentration	Humidity [% RH]	d_{pol} [Å]	n_{pol}
0.5 mol %	ambient	0.2 ± 2.0	1.3–1.5
80 mol %	11.3	22.0 ± 3.4	1.3–1.5
	33.1	27.0 ± 4.5	1.3–1.5
	75.5	37.5 ± 3.5	1.3–1.5
	85.1	40.0 ± 5.0	1.34 ± 0.05
	94.6	76.0 ± 3.5	1.34 ± 0.02
	97.6	84.4 ± 4.4	1.32 ± 0.03

[a] For thin polymer layers the refractive index does not affect the fit quality.

(80 mol %) at a high relative humidity (RH = 98 %). The small scatter of the data points in Figure 3 is an indication of the lateral homogeneity of the sample. The data for all three polymer concentrations fit well to a layer model that mainly takes into account changes in the polymer layer thickness. Namely, the more the polymer layer swells, the closer the refractive index of the polymer layer approaches the refractive index of water (see Table 2 and Figures S2 and S3 of the Supporting Information). For thin layers the refractive index of the layer is insignificant, which therefore does not allow it to be determined from the experimental data.

Figures 4 and 5 show the measured X-ray reflectivities (gray circles), the corresponding least-squares fits (black lines), and the scattering length density profiles reconstituted from the best-fit results at the lipopolymer concentrations of 6 and 80 mol %, respectively. The presence of clear features (Kiessig
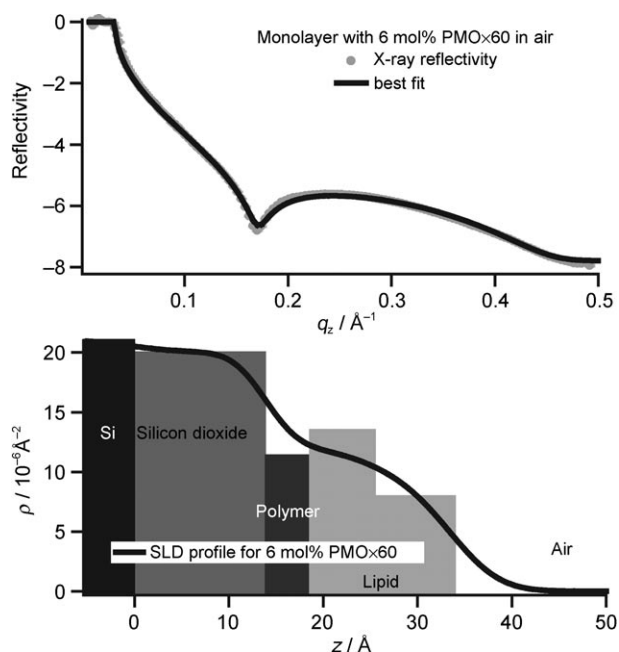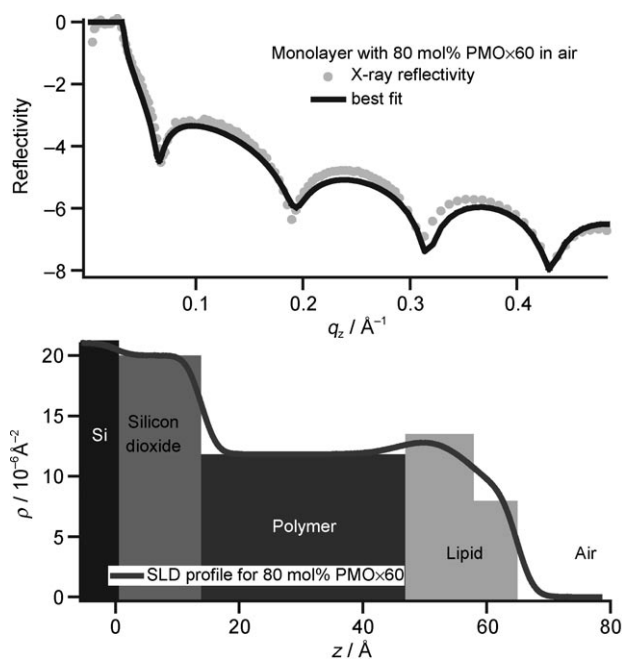
Figure 5. X-ray reflectivity measurement of a monolayer doped with 80 mol % PMOx60 on silicon substrate. Top: X-ray reflectivity data and best fitting model. Bottom: SLD profile of the best fitting model. The bars in the background correspond to the underlying layers of the SLD model.

fringes) confirms the homogeneity of the stratified structures of the transferred monolayers. The X-ray reflectivity curves of lipid–lipopolymer monolayers in air were well represented by a four-layer model which consists of a) oxide, b) polymers, c) lipid head groups, and d) hydrocarbon chains. The first two layers (silicon dioxide and polymer) are identical to the model used for ellipsometry, while the lipid layer was split into two layers corresponding to head groups and hydrocarbon chains. From the position of the Kiessig fringes in each reflectivity curve, the overall thickness of the system is well defined. If one assumes that the lipid monolayer (layers c and d) remains intact in the absence and presence of lipopolymers, the changes in the overall thickness can be attributed to the change in thickness of the polymer layer (layer b). According to the model used for the ellipsometry results (Table 1), we first assumed the scattering length density and thickness of layer c (head groups) and layer d (chains) to be $\rho_c = 13.5 \times 10^{-6}$ Å^{-2}, $d_c = 10$ Å and $\rho_d = 7 \times 10^{-6}$ Å^{-2}, $d_d = 8$ Å. The silicon dioxide was modeled with the same thickness $d_a = 13.8$ Å and scattering length density $\rho_a = 20 \times 10^{-6}$ Å^{-2} as used for ellipsometry. A lower limit for the roughness between two layers was set to 2 Å. Starting from these values, a reasonable agreement to the measured reflectivity curves was achieved. The obtained parameters for the polymer layers are summarized in Table 3. The scattering length density profiles reconstructed from these parameters are presented in the lower panels in Figures 4 and 5. At high polymer concentrations, the thickness of the lipid monolayers (layers c and d) was slightly thinner ($\Delta d \approx 3$ Å) due to the fact that the polymer head group is directly linked to the glycerol junction via a stable ether bond. However, the fit result shows no remarkable change in the

Figure 4. X-ray reflectivity measurement of a monolayer doped with 6 mol % PMOx60 on silicon substrate. Top: X-ray reflectivity data and best fitting model. Bottom: scattering length density (SLD) profile of the best fitting model. The bars in the background correspond to the underlying layers of the SLD model.

Table 3. Layer thicknesses obtained from X-ray reflectivity measurements for dry monolayers.

Concentration [mol %]	d_{pol} [Å]	ρ_{pol} [10^{-6} Å^{-2}]	σ [Å]
6	4.7	11.5	6
80	32.9	11.8	5.1

scattering length density of layer c ($\Delta\rho_c/\rho_c < 5\%$) because the scattering length density contrast at the alkyl chain/polymer interface is poorer than that at the alkyl chain/head group interface (Figures 4 and 5). Thus, changes in the global shape of the reflectivity curves can mainly be attributed to the polymer layers.

Characterization of the Bilayer in Water

Deposition of the distal layer by LS transfer avoids the potential loss of lipopolymer molecules from the proximal monolayer, which might happen upon the direct injection of vesicle suspensions onto the dry monolayer. As the first step of the characterization, the homogeneity of the polymer-tethered membranes doped with 0.2 mol % of fluorescent labeled lipid (Texas Red–DHPE; DHPE = 1,2-dihexadecanoyl-*sn*-glycero-3-phosphoethanolamine) in the distal layer was confirmed on glass slides using fluorescence microscopy. As shown in Figure 6, the polymer-tethered membranes were laterally uni-
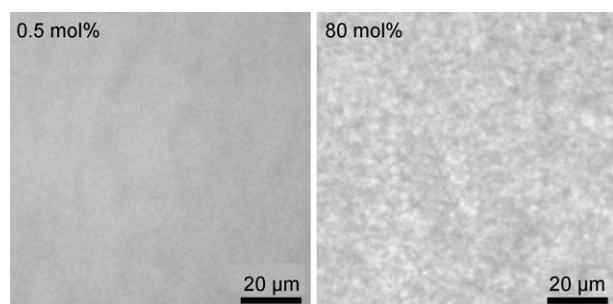
Figure 6. Fluorescence micrographs of PMOx60-doped bilayer under water. Texas Red–DHPE was used as a fluorescent marker in the proximal layer with a concentration of 0.2 mol %. The distal layer was formed by LS transfer of SOPC. Left: detail for 0.5 mol % doping ratio; right: for 80 mol % polymer content in the proximal layer.

form both at low (0.5 mol %) and high (80 mol %) lipopolymer fractions. Since the lateral diffusivity of lipid molecules is a very sensitive measure for the fluidity and continuity of the supported membrane, we calculated the lateral diffusion coefficient D of Texas Red–DHPE by the so-called continuous bleaching method.[40] At 0.5 mol % PMOx60, a diffusion coefficient of $D = 2 \, \mu m^2 s^{-1}$ was obtained. On the other hand, a 20 times smaller diffusion coefficient of $D = 0.1 \, \mu m^2 s^{-1}$ was obtained at a higher lipopolymer fraction (80 mol %). The observed tendency seems consistent with a previous report by Deverall et al., which dealt with supported membranes incorporating lipopolymer tethers with poly(2-ethyl-2-oxazoline) spacers.[41] Note

that both lipopolymers and lipids are freely diffusive, since there is no covalent link between the membrane and the glass substrate. Thus, a clear decrease in the diffusion coefficient can be interpreted in terms of the increase in the friction in the head-group region caused by the increase in the viscosity of the polymer interlayer.[42]

Thicknesses of the polymer-tethered bilayer membranes under water at different lipopolymer fractions were measured by ellipsometry. As presented in Figure 7, the increase in lipo-
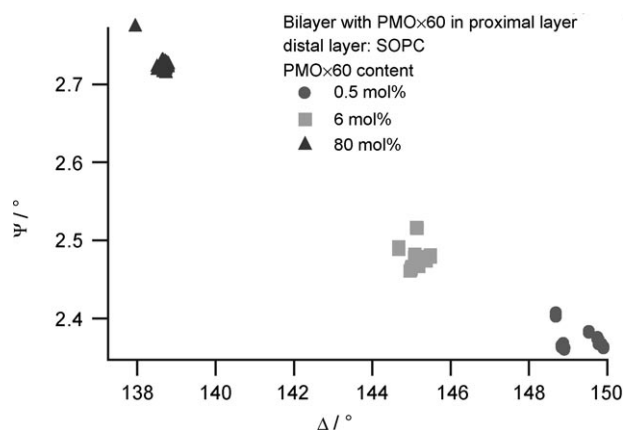
Figure 7. ψ versus Δ plot of ellipsometric measurement on a bilayer doped with PMOx60 under water on a silicon substrate. Each sample was measured at least at ten different spots. The small scatter of data shows the lateral homogeneity of the bilayer.

polymer fraction leads to a monotonic increase of ψ and a decrease of Δ. It is notable that the data points scatter much more than those measured in dry air (Figure 3). This can be explained by the amplification of inhomogeneities upon hydration of the polymer layer, which results in an increase in the roughness of the membrane.

The thicknesses of the swollen polymer layers under lipid bilayer membranes are summarized in Table 4. At the lowest lipopolymer fraction (0.5 mol %), the initial polymer layer thickness in air (0.2 Å) was very close to the resolution of our instrument. Here, we observed no clear sign to indicate the expansion of membrane–substrate spacing by the hydration of polymers. For the high lipopolymer fractions of 6 and 80 mol %, we observed an increase in polymer layer thickness by a factor of 7–10 upon complete hydration. The swelling between RH = 11 % and 97.6 % is by a factor of 3.1–4.7 for 80 mol % PMOx60, which is significantly higher than the 1.6–1.8 of PMOx30 homopolymers covalently grafted onto the substrate.[43] This difference can be due to different chain lengths and the lower lateral density of polymer chains.

Discussion

To keep a finite membrane–substrate distance, a balance must exist between all interfacial forces.[44] Herein, we consider a) van der Waals force, b) hydration repulsion, and c) undulation repulsion originating from the thermodynamic fluctuation

Table 4. Layer thicknesses and refractive indices obtained from ellipsometry measurements for bilayers under water.[a]

Concentration [mol %]	d_{pol} [Å]	n_{pol}
0.5	0	–
6	69 ± 13	1.340 ± 0.002
80	176 ± 18	1.348 ± 0.002

[a] For the lowest polymer concentration, a two-layer model is sufficient, which corresponds to a vanishing polymer layer thickness and a therefore undefined refractive index.

of the membrane. The contribution of electrostatic interactions can be excluded in our experimental system, as the polymer spacers are neutral and the phospholipids are zwitterionic.[45] The van der Waals pressure is calculated on the basis of a five-layer model as a function of the polymer layer thickness d (see the Supporting Information for details on the calculation of the van der Waals contribution).[44] Layers one and two are the bulk crystalline silicon and silicon dioxide (thickness T_1), respectively. Layer three consists of the polymer spacer, layer four is the lipid membrane with thickness T_2, and layer five is either air (monolayer) or water (bilayer). The van der Waals pressure for a five-layer model is given approximately by [Eq. (2)]:

$$P_{vdW}(d) = \frac{1}{6\pi}\left(\frac{A_{234}}{d^3} - \frac{\sqrt{A_{121}A_{343}}}{(d+T_1)^3} - \frac{\sqrt{A_{545}A_{323}}}{(d+T_2)^3} - \frac{\sqrt{A_{545}A_{121}}}{(d+T_1+T_2)^3}\right) \tag{2}$$

where A_{xyz} denotes the Hamaker constant of medium x interacting with medium z through medium y. Details of the calculation of the Hamaker constants can be found in the Supporting Information.

The hydration repulsion due to the swelling of polymer chains can be modeled by an exponential decay with distance, $P_{hyd}(d) = p_0 e^{-d/\lambda}$, parameterized by a pressure constant p_0 and a decay constant λ.[46] The values for p_0 and λ are extracted from the force–distance relationships, which were obtained by measuring the equilibrium thicknesses of the polymer layer at different osmotic pressures.[43]

Repulsive forces originating from thermodynamic undulations were first described by Helfrich.[47] For a single membrane, the pressure exerted by the fluctuation of the membrane onto adjacent walls is given by [Eq. (3)]:

$$P_{und}(d) = \alpha_1 \frac{(k_B T)^2}{\kappa d^3} \tag{3}$$

where k_B is the Boltzmann constant, T the temperature, and κ the bending rigidity of the membrane. The prefactor value $\alpha_1 = \frac{\pi^2}{128}$ has been found by analytical derivation and was confirmed by Monte Carlo simulations.[48, 49]

In Figures 8a and b, each of the three interfacial pressures and their sum are plotted versus the thickness of polymer interlayers d for polymer concentrations of 6 and 80 mol %, respectively. In both panels, the data points from the experimentally determined force–distance relationships are plotted,
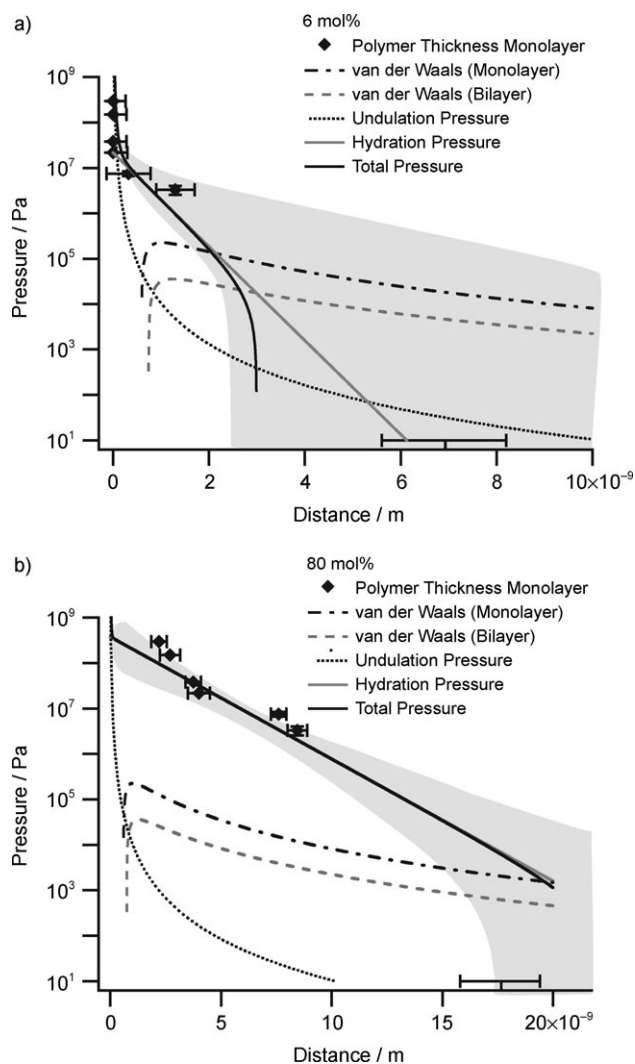
Figure 8. Polymer layer thickness measured at different osmotic pressures for 6 mol % PMOx60 (a) and 80 mol % PMOx60 (b). The contributions to the total pressure (——) are the attractive van der Waals pressure (–•–•), the undulation pressure (•••••), and the hydration pressure (gray solid line and shaded area). The van der Waals pressure is displayed with opposite sign to make a comparison possible. The polymer thickness for the bilayer under water is shown as a line above the ordinate axis.

which can be fitted with exponential functions in the hydration repulsion regime. Note that the data points above 5×10^7 Pa were not included in the fit, since the force–distance relationship in such a high-pressure regime is governed by steric repulsion due to the finite compressibility of the polymer chains.[43] As indicated by the shaded areas, the exponential fits of the measured data points yielded the characteristic parameters for each polymer fraction: $p_0 = 2.1 \times 10^7$–2.2×10^7 Pa and $\lambda = 4.8$–7.0 Å for 6 mol %, and $p_0 = 32.5 \times 10^7$–43.2×10^7 Pa and $\lambda = 15.2$–17.2 Å for 80 mol %.

At the lipopolymer fraction of 6 mol % (Figure 8a), the extrapolation of the sum of the aforementioned three pressures to zero predicts the equilibrium distance of about 3–10 nm, which shows good agreement with the polymer layer thickness obtained by ellipsometry (Table 4). As presented in Figure 8b, the scatter of the data points at higher humidity is more

pronounced at the lipopolymer fraction of 80 mol%. The range of the equilibrium thickness calculated for the zero-pressure condition is around 21 nm, thus showing the experimentally determined equilibrium polymer thickness [(176 ± 18) Å] to be limited by the stretched polymer length (≈ 180 Å). Apart from this limit the calculation suggests that the equilibrium thickness of the membrane–substrate distance maintained by the polymer spacers can quantitatively be explained in terms of the interplays of three major interfacial forces.

One of the main advantages of the successive deposition of the monolayers onto a membrane is the capability to precisely control the lateral density of lipopolymer tethers in asymmetric membranes. Here, the volume occupied by one polymer chain can be calculated from the lateral density of the polymer chains and the experimentally determined polymer layer thickness. Since such a calculation becomes erroneous at lower lipopolymer fractions where the errors in the layer thickness are comparable to the absolute values (Table 2), we focus on discussion of the case of the highest lipopolymer content (80 mol%). For example, the area per polymer chain at a lateral pressure of $p = 30$ mN m^{-1} can be obtained from the pressure–area isotherm (see Supporting Information) to be $A_{polymer} = 166$ Å^2. Taking the polymer layer thickness from X-ray reflectivity in an ambient atmosphere, $d_{refl} = 32.9$ Å, the corresponding chain volume $V_{exp/ell} = 5461$ Å^3 can be calculated.

To estimate the volume fraction of hydrating water, these volumes obtained by experiment were compared to the volume predicted by the calculation method proposed by Connolly.[50] Using a probe radius of 1.4 Å for water, the excluded volume of one dry PMOx60 chain can be calculated to be $V_{Connolly} = 5140$ Å^3. Comparison with the experimental chain volume at RH = 85% suggests that the volume increases by 6% due to the uptake of water. However, the calculation of polymer chain volume failed under dry conditions. For example, the chain volume calculated from the thickness measured by ellipsometry at RH = 11.3%, $V_{exp/ell} = 3652$ Å^3, is much smaller than $V_{Connolly}$. This discrepancy suggests that the polymer layer thickness is underestimated in our slab model. One possible scenario would be that polymer chains are partially immersed in layer c representing the head groups of phospholipids. This actually seems reasonable since polymer chains are directly connected to the glycerol junction via ether bonds. In fact, if one assumes that approximately 80% of layer c with a thickness of 11 Å is filled with polymers, the expected volume of 1461 Å^3 agrees very well with the difference $V_{Connolly} - V_{exp/ell} = 1488$ Å^3.

After the deposition of the distal monolayer, the polymer layer now under bulk water becomes thicker by a factor of 6 ($d_{exp/ell} = 176$ Å), which corresponds to $V_{exp/ell} = 29216$ Å^3. Here, the influence of the polymer immersed in layer c on the entire volume of polymer is merely 5%, and the volume fraction of water, $\Phi_{water/ell} = 82\%$ (5140/29216 ≈ 0.18) is obtained. This value is larger than those reported for a supported membrane tethered with short hexa(ethylene oxide) spacers using neutron reflectivity: $\Phi_{water/neu} = 4\%$ for membranes with 100 mol% tethers, and 50–60% for 50 mol% tethers.[51] A distinct difference in the degrees of hydration suggests that longer poly(2-oxazoline) head groups can take up more water than oligo(ethylene oxide) head groups possessing much fewer conformational degrees of freedom.[10,52]

Conclusions

The main thrust of this paper is to highlight the influence of lipopolymer fractions on vertical structures and substrate–membrane interactions. Further studies on the effect of polymer chain lengths at a fixed lateral density will unravel the effect of polymer chain lengths in a complementary manner. Currently, we are carefully optimizing the sample environments for high-energy specular X-ray reflectivity at the solid/liquid interface ($E > 20$ keV). Additionally, neutron reflectivity is specifically suited for structural characterization of bilayers in bulk water owing to the high scattering length density contrast available by deuteration.[25] Thus, the combination of ellipsometry, X-ray reflectivity, and neutron reflectivity would serve as a powerful tool for quantitative characterization of model membranes on soft polymer supports, to reveal the generic roles of hydrated polymers in the fine adjustment of cell–cell and cell–matrix interactions in nature.

Keywords: ellipsometry · interfaces · lipopolymers · membranes · X-ray reflectivity

[1] E. Sackmann, *Science* **1996**, *271*, 43–48.
[2] A. A. Brian, H. M. McConnell, *Proc. Natl. Acad. Sci. USA* **1984**, *81*, 6159–6163.
[3] J. T. Groves, *Angew. Chem.* **2005**, *117*, 3590–3605; *Angew. Chem. Int. Ed.* **2005**, *44*, 3524–3538.
[4] M. Tanaka, E. Sackmann, *Nature* **2005**, *437*, 656–663.
[5] M. Tanaka, *MRS Bull.* **2006**, *31*, 513–520.
[6] E. Sackmann, M. Tanaka, *Trends Biotechnol.* **2000**, *18*, 58–64.
[7] H. Lang, C. Duschl, H. Vogel, *Langmuir* **1994**, *10*, 197–210.
[8] M. L. Wagner, L. K. Tamm, *Biophys. J.* **2000**, *79*, 1400–1414.
[9] N. Bunjes, E. K. Schmidt, A. Jonczyk, F. Rippmann, D. Beyer, H. Ringsdorf, P. Gräber, W. Knoll, R. Naumann, *Langmuir* **1997**, *13*, 6188–6194.
[10] O. Purrucker, A. Förtig, R. Jordan, M. Tanaka, *ChemPhysChem* **2004**, *5*, 327–335.
[11] B. A. Cornell, V. L. B. Braach-Maksvytis, L. G. King, P. D. J. Osman, B. Raguse, L. Wieczorek, R. J. Pace, *Nature* **1997**, *387*, 580–583.
[12] S. M. Schiller, R. Naumann, K. Lovejoy, H. Kunz, W. Knoll, *Angew. Chem.* **2003**, *115*, 219–222; *Angew. Chem. Int. Ed.* **2003**, *42*, 208–211.
[13] O. Purrucker, A. Förtig, R. Jordan, E. Sackmann, M. Tanaka, *Phys. Rev. Lett.* **2007**, *98*, 078102.

[14] R.-J. Merath, U. Seifert, *Phys. Rev. E* **2006**, *73*, 010401(R).

[15] A. Lambacher, P. Fromherz, *Appl. Phys. A* **1996**, *63*, 207–216.

[16] V. Kiessling, L. K. Tamm, *Biophys. J.* **2003**, *84*, 408–418.

[17] D. Braun, P. Fromherz, *Phys. Rev. Lett.* **1998**, *81*, 5241–5244.

[18] L. Y. Hwang, H. Götz, W. Knoll, C. J. Hawker, C. W. Frank, *Langmuir* **2008**, *24*, 14088–14098.

[19] C. Striebel, A. Brecht, G. Gauglitz, *Biosens. Bioelectron.* **1994**, *9*, 139–146.

[20] G. Puu, I. Gustafson, *Biochim. Biophys. Acta, Biomembr.* **1997**, *1327*, 149–161.

[21] M. C. Howland, A. W. Szmodis, B. Sanii, A. N. Parikh, *Biophys. J.* **2007**, *92*, 1306–1317.

[22] E. Nováková, K. Giewekemeyer, T. Salditt, *Phys. Rev. E* **2006**, *74*, 051911.

[23] C. E. Miller, J. Majewski, T. Gog, T. L. Kuhl, *Phys. Rev. Lett.* **2005**, *94*, 238104.

[24] M. B. Hochrein, C. Reich, B. Krause, J. O. Rädler, B. Nickel, *Langmuir* **2006**, *22*, 538–545.

[25] F. Rehfeldt, R. Steitz, S. P. Armes, R. von Klitzing, A. P. Gast, M. Tanaka, *J. Phys. Chem. B* **2006**, *110*, 9171–9176.

[26] T. Schubert, P. C. Seitz, E. Schneck, M. Nakamura, M. Shibakami, S. S. Funari, O. Konovalov, M. Tanaka, *J. Phys. Chem. B* **2008**, *112*, 10041–10044.

[27] *Lipid Bilayers: Structure and Interactions* (Eds.: J. Katsaras, T. Gutberlet), Springer, Berlin, **2001**.

[28] R. M. A. Azzam, N. M. Bashara, *Ellipsometry and Polarized Light*, North-Holland, Amsterdam, **1987**.

[29] O. Purrucker, S. Gönnenwein, A. Förtig, R. Jordan, M. Rusp, M. Bärmann, L. Moroder, E. Sackmann, M. Tanaka, *Soft Matter* **2007**, *3*, 333–336.

[30] W. Kern, D. A. Puotinen, *RCA Rev.* **1970**, 187–206.

[31] R. Jordan, K. Graf, H. Riegler, K. K. Unger, *Chem. Commun.* **1996**, 1025–1026.

[32] R. Jordan, K. Martin, H. J. Räder, K. K. Unger, *Macromolecules* **2001**, *34*, 8858–8865.

[33] P. Persigehl, R. Jordan, O. Nuyken, *Macromolecules* **2000**, *33*, 6977–6981.

[34] A. Förtig, R. Jordan, K. Graf, G. Schiavon, O. Purrucker, M. Tanaka, *Macromol. Symp.* **2004**, *210*, 329–338.

[35] O. Purrucker, A. Förtig, K. Lüdtke, R. Jordan, M. Tanaka, *J. Am. Chem. Soc.* **2005**, *127*, 1258–1264.

[36] L. Greenspan, *J. Res. Natl. Bur. Stand. A: Phys. Chem.* **1977**, *81A*, 89–96.

[37] A. Nelson, *J. Appl. Crystallogr.* **2006**, *39*, 273–276.

[38] E. D. Palik, *Handbook of Optical Constants of Solids*, Academic Press, New York, **1985**.

[39] D. Ducharme, J.-J. Max, C. Salesse, R. M. Leblanc, *J. Phys. Chem.* **1990**, *94*, 1925–1932.

[40] C. Dietrich, R. Merkel, R. Tampé, *Biophys. J.* **1997**, *72*, 1701–1710.

[41] M. A. Deverall, E. Gindl, E.-K. Sinner, H. Besir, J. Ruehe, M. J. Saxton, C. A. Naumann, *Biophys. J.* **2005**, *88*, 1875–1886.

[42] R. Merkel, E. Sackmann, E. Evans, *J. Phys. France* **1989**, *50*, 1535–1555.

[43] F. Rehfeldt, M. Tanaka, L. Pagnoni, R. Jordan, *Langmuir* **2002**, *18*, 4908–4914.

[44] J. N. Israelachvili, *Intermolecular and Surface Forces*, Academic Press, San Diego, **1991**.

[45] A. Wurlitzer, E. Politsch, S. Huebner, P. Krüger, M. Weygand, K. Kjaer, P. Hommes, O. Nuyken, G. Cevc, M. Lösche, *Macromolecules* **2001**, *34*, 1334–1342.

[46] S. Leikin, V. A. Parsegian, D. C. Rau, R. P. Rand, *Annu. Rev. Phys. Chem.* **1993**, *44*, 369–395.

[47] W. Helfrich, *Z. Naturforsch.* **1978**, *33a*, 305–315.

[48] M. Bachmann, H. Kleinert, A. Pelster, *Phys. Rev. E* **2001**, *63*, 051709.

[49] G. Gompper, D. M. Kroll, *Europhys. Lett.* **1989**, *9*, 59–64.

[50] M. L. Connolly, *J. Appl. Crystallogr.* **1983**, *16*, 548–558.

[51] D. J. McGillivray, G. Valincius, D. J. Vanderah, W. Febo-Ayala, J. T. Woodward, F. Heinrich, J. J. Kasianowicz, M. Lösche, *Biointerphases* **2007**, *2*, 21–33.

[52] S. Huber, N. Hutter, R. Jordan, *Colloid Polym. Sci.* **2008**, *286*, 1653–1661.